Photodsintegration of transversely polarised deuterons

D.P.Watts, M. Bashkanov and M. Ostrick for A2

February 2020

1 Abstract of physics

We propose to obtain new constraints on the electromagnetic properties of the recently discovered $d^*(2380)$-hexaquark utilising a transversely polarised deuteron target and a polarised photon beam. A set of single- and double-polarision observable determination will underpin determination of the photo-coupling of the d^* to the deuteron as well as providing new constraints on the d^* electric quadrupole and magnetic octupole deformations. The measurement has potential impact not only to the emerging field of multiquark states in hadron physics but also to astrophysics, where the $d^*(2380)$ has the potential to play a crucial role in neutron stars.

2 Abstract of experiment

The experiment will be performed at the MAMI tagged photon facility (Glasgow/Mainz Tagger) using the Crystal Ball/TAPS detector setup, together with particle identification detector (PID) and multi-wire proportional chambers (MWPCs). An elliptically polarised photon beam with coherent edge around 630 MeV will be used in conjunction with a transversely polarised deuteron target. Additional "empty target" runs will be also carried out to verify the detector performance.

MAMI Specifications :
beam energy: 855 MeV
beam polarization: helicity polarised

Beam Specifications :
tagged energy range: 300 – 800 MeV
photon beam polarization: Linearly and circularly polarised (coherent edge 630 MeV); unpolarized.

Equipment Specifications :
detectors: Crystal Ball/TAPS, PID, MWPCs
target: polarised deuteron target

Beam Time Request :
set-up/test with beam: 1 week
data taking: 6 weeks

List of participating authors:

- **Institut für Physik, University of Basel, Switzerland**
  D. Ghosal, N. Jermann, B. Krusche, A. Kaeser, C. Meier
- **Institut für Experimentalphysik, University of Bochum, Germany**
  G. Reicherz
- **Helmholtz–Institut für Strahlen- und Kernphysik, University of Bonn, Germany**
  F. Afzal, R. Beck, A. Thiel, Y. Wunderlich
- **JINR, Dubna, Russia**
  N.S. Borisov, I. Gorodnov, A. Lazarev, A. Neganov, Yu.A. Usov
- **SUPA School of Physics and Astronomy, University of Glasgow, UK**
  S. Gardner, K. Livingston, I.J.D. MacGregor
- **Racah Institute of Physics, Hebrew University of Jerusalem, Israel**
  G. Ron
- **Kent State University, Kent, USA**
  D.M. Manley
- **Institut für Kernphysik, University of Mainz, Germany**
  P. Achenbach, M. Biroth, F. Cividini, A. Denig, P. Drexler, M.I. Ferretti-Bondy, W. Gradl, L. Heijkenskjöld, V.L Kashevarov, P.P. Martel, E. Mornacchi, M. Ostrick, V. Sokhoyan, C. Sfienti, M. Thiel, A. Thomas, S. Wagner, J. Wettig
- **University of Massachusetts, Amherst, USA**
  R.Miskimen
- **Institute for Nuclear Research, Moscow, Russia**
  G. Gurevic
- **INFN Sezione di Pavia, Pavia, Italy**
  A. Braghieri, S. Costanza, P. Pedroni
- **Department of Physics, University of Regina, Canada**
  G.M. Huber
- **Mount Allison University, Sackville, Canada**
  D. Hornidge
- **George Washington University, Washington, USA**
  W.J. Briscoe, E.J. Downie, I.I. Strakovsky
- **Department of Physics, University of York, UK**
  M. Bashkanov, S. Fegan, D.P. Watts, D. Werthmüller, N. Zachariou
- **Rudjer Boskovic Institute, Zagreb, Croatia**
  M. Korolija

3 Introduction

The photodisintegration of the deuteron is one of the simplest reactions in nuclear physics, in which a well understood and clean electromagnetic probe leads to the breakup of a few-body nucleonic system. However, despite experimental measurements of deuteron photodisintegration spanning almost a century [1], many key experimental observables remain unmeasured, or have been only measured in rather limited or coarse kinematics. This is particularly evidenced at distance scales (photon energies) where the quark substructure of the deuteron can be excited. This limits a detailed assessment of the reaction mechanism, including the contributions of nucleon resonances, meson exchange currents as well as constraining roles for more exotic QCD possibilities, such as the six-quark containing (hexaquark) $d^*(2380)$. The $d^*(2380)$ was recently evidenced in a range of nucleon-nucleon scattering reactions [2, 3, 4, 5, 6, 7, 8, 9]. The $d^*(2380)$ has inferred quantum numbers $I(J^P) = 0(3^+)$ and a mass $\sim$ 2380 MeV, which in photoreactions would correspond to a pole at $E_\gamma \sim 570$ MeV. Confirmatory evidence for the existence of the $d^*(2380)$ with different probes, along with new access to key properties (e.g. electromagnetic coupling of the $d^*(2380)$) would have important ramifications for the emerging field of non-standard multiquark states and also our understanding of the dynamics of condensed matter systems such as neutron stars [11]. Recent works on deuterium photodisintegration at MAMI have shown sensitivities to a d^* contribution in the beam spin asymmetry [45] and most recently in the final state nucleon polarisation [14]. In this proposal we will obtain the first measurements of polarised beam-transverse target asymmetries for photon energies below, through, and above the d^* region. This unique dataset will provide powerful information on the mechanisms of deuterium photodisintegration, including the contribution of d^* and constraints on background processes.

3.1 d^* in the context of the wider programme in multiquark states

The investigation of multiquark states (by which we mean non-standard states beyond the 2q and 3q systems) and many-body interactions within the theory of strong interaction, (Quantum ChromoDynamics (QCD)) is a major challenge for contemporary experimental and theoretical physics. Currently, little is known in detail about multiquark states. A plethora of states have recently been obtained in high energy experiments in the heavy quark sectors, where the production of multiquark states allows more straightforward separation from their conventional partners. Unfortunately, the majority of these heavy-quark multiquark states are expected to be "trivial" hadronic molecules with two colour bags separated by a distance of up to few fermi's. In addition, production of multiquark states with good statistics is rather difficult. Because of this the quantum number determination, determination of the complete branching ratios, and shape/structure determination for these states is challenging.

The light-quark sector offers certain advantages: due to the lower centre-of-mass energy required for production, such states can be produced more copiously, and are more amenable to measurement in photo/electroproduction. This provides potential access to the size/structure of a multiquark state and also benefits from the clean production environment of electromagnetic probes. Compared to other light multiquark states, hexaquarks with baryon number $B = 2$ (dibaryons) are appealing as they are separable from conventional 2q/3q states. The d^* is the only known state which is predicted to be a "genuine hexaquark" state by several chiral quark models and which also has some indications of compact hexaquark-like signatures from recent experimental data[45]. It is well separated in terms of quantum numbers and predicted properties from the more trivial baryon-baryon molecular states e.g. the deuteron.

3.2 Astrophysical implications of d^*

The role of a $d^*(2380)$ degree of freedom for the nuclear equation of state, EoS ([10]) was recently studied in several papers [11, 12]. The $d^*(2380)$ is a massive positively charged non-strange particle with integer spin (J=3) and is the first predicted non-trivial hexaquark supported by experiment ([3, 4, 8]). The importance of such a new degree-of-freedom resides in the fact that it has the same u, d quark composition as neutrons and protons and, therefore, does not involve any strangeness degrees of freedom. Moreover, it is a boson and as such, has the possibility to condense within neutron stars. It was shown that despite its large mass, the $d^*(2380)$ can appear in the neutron star (NS) interior at densities similar to those predicted for the appearance of other proposed states e.g. nucleon resonances, Δ's, or hyperons. The effect of the $d^*(2380)$ on the nuclear equation of state (EoS) was studied both in non-interacting and interacting cases (both attractive and repulsive). The results indicate the $d^*(2380)$ has the potential to be an important new degree of freedom in neutron stars. Fractions of $d^*(2380)$ of around 20% are predicted in the centre of heavy stars, resulting

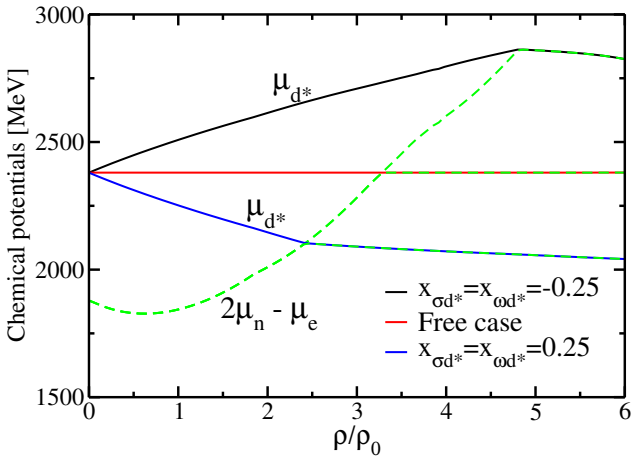

Figure 1: Chemical equilibrium condition for the appearance of the $d^*(2380)$ hexaquark in β-stable matter. Results are shown for the cases in which the $d^*(2380)$ feels attraction ($x_{\sigma d^*} = x_{\omega d^*} = 0.25$), repulsion ($x_{\sigma d^*} = x_{\omega d^*} = -0.25$) or does not interact at all with the rest of the particles of the system.

in an increased maximum star radius and a reduced central density. New neutrino and antineutrino cooling mechanisms are possible with $d^*(2380)$ formation, which have previously not been included in neutron star modelling. The EoS with explicit $d^*(2380)$ degrees of freedom is one of the few which predict NS mass-radius relation consistent with the latest (subsequent) gravitational wave experimental results [13]. Indeed, the presence of the $d^*(2380)$ is predicted to set a strict limit on a maximum neutron star mass in agreement with that inferred from gravitational wave data [11, 12]. As an isoscalar particle the interaction of the d^* is reduced to isoscalar (dominantly σ, ω) exchanges. Interplay between the $d^*(2380)$ dimensionless coupling constants ($x_{\sigma d^*} = \frac{g_{\sigma d^*}}{g}$, $x_{\omega d^*} = \frac{g_{\omega d^*}}{g_{\omega N}}$) and its chemical potential in neutron star matter are shown on Fig. 1. As expected, an attractive interaction between the d^*'s and the nuclear matter leads to earlier appearance of the d^* (in terms of nuclear density) in nuclear matter and a stronger reduction of the fractional protons and neutron composition [12]. The EoS and corresponding NS mass-radius relation in presence of the d^* can be seen on Fig. 2.

Furthermore, it was recently indicated that the Bose-Einstein condensates of the d^*-hexaquarks could be produced copiously in early universe and might contribute to a dark matter, Fig. 3, see Ref. [15] for details. From these, it is clear that the extraction of the d^* properties, such as it size, structure, magnetic moment, quadrupole deformation, photo coupling (which can be related to an $x_{\omega d^*}$ in a vector meson dominance model and hence to a strength of the d^* repulsive term) have strong potential impact for astrophysics as well as for hadron and strong interaction physics.

3.3 Photoproduction of the d^*

The d^* is a $I(J^P) = 0(3^+)$ sate, hence it can be photoproduced from the deuteron via three possible multipole transitions - $E2, M3$ or $E4$. These transitions are proportional to the electric transition quadrupole moment, $Q_{d \to d^*}$, to the magnetic transition octupole moment, $\Omega_{d \to d^*}$, and to the electric transition decupole moment $D_{d \to d^*}$, respectively [16]. The $E4$ transition is expected to be highly suppressed, and therefore we assume in all subsequent chapters that only $E2$ and $M3$ transitions contribute (unless otherwise explicitly stated). The proposal is organised as follows: after a theoretical introduction (Chapter 4) which links experimental observables with production amplitudes, we outline the experimental apparatus (Chapter 5), discuss the analysis methods (Chapter 6), and finally evaluate required beamtime (Chapter 7).

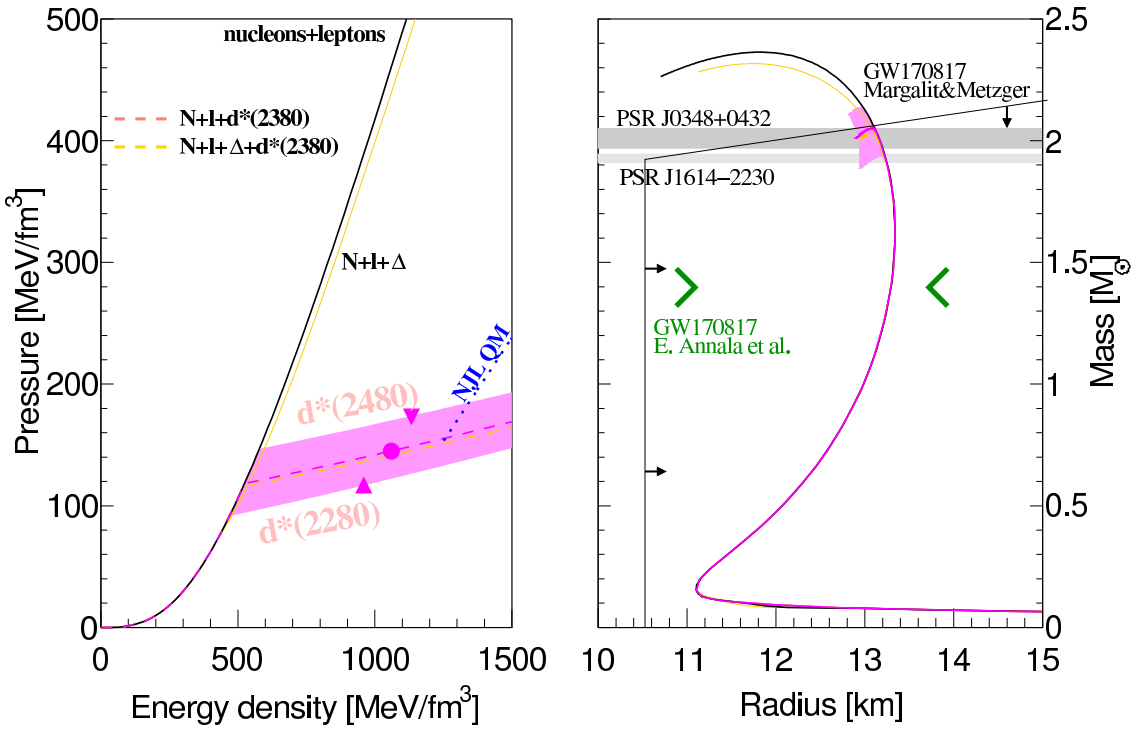

Figure 2: Neutron star EoS (left) and mass-radius relation (right) with and without the d^* degree of freedom. The predictions assuming $m_{d^*} = [2280, 2480]$ MeV and $m_{d^*} \equiv 2380$ MeV are shown by the shaded bands and dashed pink lines respectively. The effect of the Δ degree of freedom is shown as a gold line with $d^*(2380)$(dashed) and without (solid). The observational masses of the pulsars PSR J1614-2230 ($1.928 \pm 0.017 M_\odot$) [21] and PSR J0340+0432 ($2.01 \pm 0.04 M_\odot$) [22] as well as neutron star merger GW170817 limits from [13] and [23] are also shown. The pink markers on a left panel represent the maximum achievable pressure/energy density for heavy neutron star with d^* degrees of freedom for the $m_{d^*} = 2380$ MeV(circle), 2280 MeV and 2480 MeV(triangles). Pure NJL quark matter EoS is shown by dashed blue line.

4 Current status - theory and experiment

Theoretical models of deuterium photodisintegration including the d^* degree of freedom are currently under development at MAMI [53], resulting in a crucial need to obtain experimental data to challenge these new developments. Key to fully establishing the d^* photoproduction is the consistency of its signal (or lack of signal) in different observables. Suitable predictions will be available for the analysis and interpretation of the proposed data, but are not currently at a stage to be exploited in the proposal. However, the proposed timeline of the measurement is crucial to provide data in a timely fashion for these developments.

It has been shown in many recent measurements from MAMI, ELSA, JLAB, LEPS how polarisation observables are indespensible in photoproduction reactions to extract information on sub-dominant contributions and provide better constraints on the underlying reaction amplitudes. Reaction processes can be evidenced in interference effects in polarisation observables, even when giving small signals in the total or differential cross sections. The nature of background processes can also be suppressed or established in more detail, utilising the accessible spins for different orientations of beam and target spin.For example, with beam-target observables the $N^*(1520)$ resonance(which has a dominant contribution in single pion photoproduction in the "second resonance" region) can be effectively suppressed if one anti-aligns the relative polarisations between the photon and the target. The contribution of background channels to the d^* in deuterium, photodisintegration (e.g. N* production) can be enhanced/suppressed for different polarisation observables.

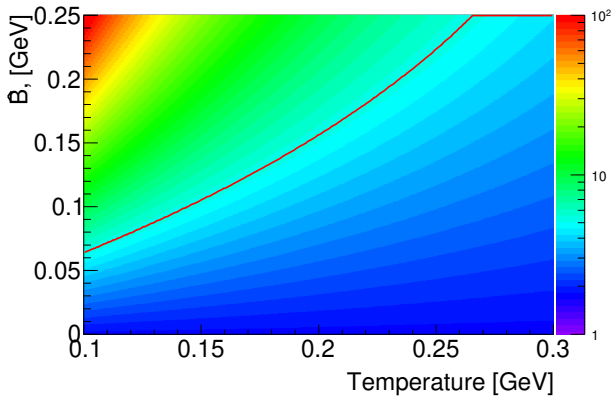

Figure 3: The primordial production of $d^*(2380)$-BEC (expressed as a ratio to baryon matter) calculated as a function of binding energy per baryon, $\hat{B}$ and matter-dark matter decoupling temperature. The red line shows the loci corresponding to the current experimental determination of the dark matter to matter ratio[**?**].

4.1 Summary of previous measurements/analysis

Although there are no measurements of beam-target observables for deuterium photodisintegration in the region of the d^*, there are a number of recent results utilising polarised/unpolarised gamma beams and recoil polarisation which have given first information on the role of the d^*. In $\gamma d \to d\pi^0\pi^0$ measurements of Refs. [24] and [25], a structure in the region of the d^* with properties consistent with those extracted from the previous NN scattering experiments is observed. The strength of the $(\gamma d \to d^* \to d\pi^0\pi^0)$ contribution is estimatyed to be of the order of 30 nb. Since the branching ratios of $\frac{Br(d^*\to pn)}{Br(d^*\to d\pi^0\pi^0)} = \frac{12(3)\%}{14(1)\%} \sim 1$, one can expect a similar d^* contributions in the deuteron photodisintegration channel. These cross section evaluations of the d^* contribution are compatible with the properties of the structures observed from truncated PWA analysis of the beam polarisation asymmetry (Σ), (see discussion in Ref. [45]). From these prior results, the total cross section of $\gamma d \to pn$ reaction in the region of the d^* was inferred to be $3-5\mu b$, which is dominated by the tails of Δ and $N^*(1520)$ resonances.

In our proposal we focus on the photodisintegration reaction as the two body final state is more amenable to PWA than the $\gamma d \to d\pi^0\pi^0$ (however data from this reaction will also be recorded and studied in parallel). Very recently beam-recoil observables have been determined in deuterium photodisintegration in the region of the d^*. There was a long standing anomoly in the induced polarisation of the proton (p_y^p), where the polarisation reaches around 100% in the region of the d^*. Such behaviour could not be explained using models which included only N^* degrees of freedom. Our recent measurement [14] of the final state neutron polarisation revealed mirror behaviour, currently not described by conventional theory, is also evident in (p_y^n) (see Fig. 5), adding further intrigue to this puzzle. As shown in Fig. 5 the inclusion of a phenomenological d^* contribution with properties established from the prior NN scattering experiments is a plausible explanation of this effect in both p_y^p and p_y^n. We note the induced recoil observables reflect the imaginary parts of the reaction amplitudes (See subsequent discussion and Table 2). Further, preliminary evaluations of transferred polarisation, C_x (which reflects the real parts of the same photoproduction amplitudes as for the induced polarisations) exhibits a zero crossing close to the pole of the d^*.

There have been previous measurements of deuterium photodisintegration from transversely polarised targets. The T single polarisation observable ($T = \frac{3}{2}\frac{\sigma_{\Uparrow}-\sigma_{\Downarrow}}{\sigma_{\Uparrow}+\sigma_{\Downarrow}+\sigma_{\odot}}$) has been extracted, albeit in rather large 100 MeV photon energy bins, which a resulting reduced sensitivity to narrow features such as the d^*. However, already in these analysis it was indicated that there was anomolous structure in the gamma energy bin containing the d^* (See Fig 5). In analysis of the angular distribution of the measured target asymmetry observable the need for a higher multipole contribution in the bin conataining the d^* was already indicated. Such effects would be consistent with a role for d^* excitation, which as discussed earlier proceeds via higher multipoles. Clearly, more accurate data in finer gamma bins would help elucidate the nature of this anomoly and enable first determination whether it shows charactersitics (e.g. width) compatible with the known properties of the d^*. It should be remarked that these previous measurements (derived from an asymmetry

in the yields between opposite orientations of the transverse polarisation) include additional contribution from the tensor asymmetry ($\sigma_{\odot}$) which does not fully cancel for a spin 1 target (although its effects were taken as small and included in the systematic error - see Ref [55] for a discussion). In case of 75% of vector polarisation we expect about 40% of tensor polarisation for our target. With the proposed measurement we can utilise the existing unpolarised Deuterium CB data set from our previous measurement (and employ common analysis cuts) to obtain the unpolarised cross section ($= \sigma_{\Uparrow} + \sigma_{\Downarrow} + \sigma_{\odot}$) and better account for any residual tensor component.

Clearly, from all these prior measurements, there are strong suggestions of the d^* playing a role in deuterium photodisintegration, but it is crucial that a larger database of observables, with appropriate gamma binning to elucidate narrow structures and which constrain more of the complex reaction amplitudes is crucial for progress. MAMI is in an internationally leading position to deliver this data. The proposed target and beam-target observables can be obtained with greatly improved statistical and systematic uncertainties than achievable with the only other double-polarisation measurement with recoil polarisation (C_x).

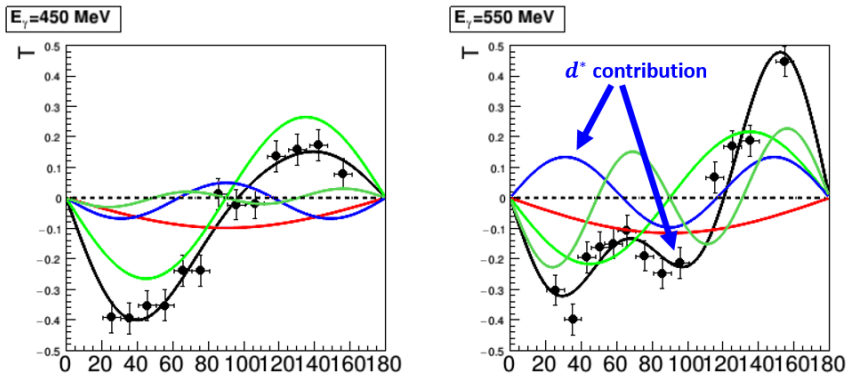

Figure 4: T observable for the $\gamma d \to pn$ reaction together with Legendre polynomial decomposition. An effect of d^* is seen at $E_\gamma \sim 550$ MeV as pronounced deep at 90°.

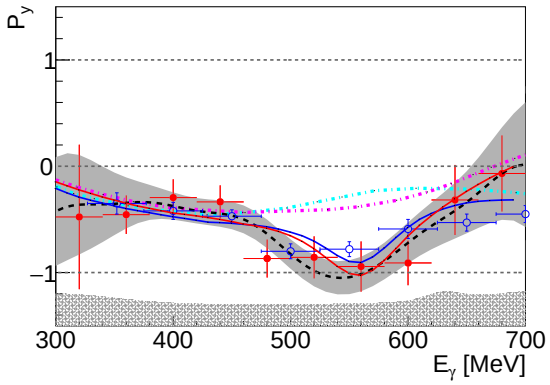

Figure 5: P_y^n (Red filled circles) and P_y^p (blue open circles) for CM angular bins centred on 90° as a function of photon energy. The result of an unbinned analysis of P_y^n is presented as black dashed line with the error bars as a grey band. The dashed-dot lines shows predictions from Ref [41] for P_y^p (cyan) and P_y^n(pink). The solid lines show the result of the fit with an additional $d^*(2380)$ contribution (see text) for P_y^p (blue) and P_y^n (red). Systematic uncertainties for the P_y^n data are shown by the hatched area.

Table 1: Deuteron photodisintegration amplitudes $t_{s,m_s,\lambda_\gamma,m_d} =< S_{pn}, M_{pn}|T|\lambda_\gamma, m_d >$ (see text for explanation of symbols)

$t_{s,m_s,\lambda_\gamma,m_d}$	S_{pn}	m_{pn}	λ_γ	m_d
$t_{1,+1,1,1}$	1	$\uparrow$	1	$\Uparrow$
$t_{1,0,1,1}$	1	0	1	$\Uparrow$
$t_{1,-1,1,1}$	1	$\downarrow$	1	$\Uparrow$
$t_{1,+1,1,0}$	1	$\uparrow$	1	$\odot$
$t_{1,0,1,0}$	1	0	1	$\odot$
$t_{1,-1,1,0}$	1	$\downarrow$	1	$\odot$
$t_{1,+1,1,-1}$	1	$\uparrow$	1	$\Downarrow$
$t_{1,0,1,-1}$	1	0	1	$\Downarrow$
$t_{1,-1,1,-1}$	1	$\downarrow$	1	$\Downarrow$
$t_{0,0,1,1}$	0	0	1	$\Uparrow$
$t_{0,0,1,0}$	0	0	1	$\odot$
$t_{0,0,1,-1}$	0	0	1	$\Downarrow$

4.2 Deuterium photodisintegration - reaction amplitudes

The deuteron photodisintegration reaction can be described in terms of 12 reaction amplitudes (Table. 1), expressed as $t_{s,m_s,\lambda_\gamma,m_d} =< S_{pn}, M_{pn}|T|\lambda_\gamma, m_d >$, where s is the combined pn spin, m_s is the third projection of pn spin, λ_γ is the photon polarisation and m_d is the 3rd projection of the deuteron polarisation. In the differential cross section the reaction amplitudes contribute as a squared sum (equation 1)

$$\frac{d\sigma}{d\Omega} = \frac{1}{3} \sum_{s,m_s,m_d} |t_{s,m_s,1,m_d}|^2 \tag{1}$$

Due to angular momentum conservation, in the case of $d^* \rightarrow pn$, the polarisation directions of neutron and proton need to be aligned. From Refs [8, 9] we know that in 90% of cases the d^* decays into ${}^3D_3$ partial wave and in 10% cases via the ${}^3G_3$ partial wave. This limits us to a contribution of functions $t_{1,m_s,1,m_d}$. In a simplified manner one can also take that $E2$ excitation of the d^* should be predominantly seen in $t_{1,m_s,1,1}$; $M3$ in $t_{1,m_s,1,0}$; and $E4$ in $t_{1,m_s,1,-1}$. The relationship between the various single and double polarisation observables in deuterium photodisintegration and the corresponding reaction amplitudes is summarised in Table. 2. Note that the d^* containing amplitudes discussed above will give contribution to all the listed observables.

Theoretical calculations for the d^* contribution in deuterium photodisintegration to various double polarisation observables are currently in development, so it is currently difficult to determine *a priori* which beam-target observables would show the most sensitivity to a d^* contribution. The existing data on single polarisation variables P_y and T (both related to imaginary part of amplitudes - see Table 2) show pronounced effects in the region of the d^* (see Fig. 5 and Fig. 4). To improve the situation regarding constraint of d^* in photoreactions we therefore wish to optimise the new measurements to constrain imaginary components of the reaction amplitudes. This leads to the conclusion that this first measurement should utilise transverse target polarisation with elliptically polarised (linear and circular) photons, which will give access to the T and T_{11}/T_{1-1} observables (Table 2) which both give information on imaginary components of amplitudes. We note that, as discussed above, the T observable already suggests interesting features in the region of the d^*. The measurement will also give access to F, which gives a new constraint on the real parts of the amplitude combinations in Table 2).

As pointed out earlier the theoretical model for deuterium photodisintegration including d^* degrees of freedom is currently under development. As an indication that high multipole mechanisms, as expected for the d^*, will manifest in our beam-target observables we discuss results from the analagous N^* sector, specifically

Table 2: Deuterium photodisintegration, selected polarisation observables

observable	amplitudes
$\frac{d\sigma}{d\Omega}$	$\frac{1}{3}\sum_{s,m_s,m_d}\|t_{s,m_s,1,m_d}\|^2 = \sigma_0(\Theta)$
Σ	$\frac{1}{3}\sum_{s,m_s,m_d}(t^*_{s,m_s,1,m_d}t_{s,m_s,-1,m_d})/\sigma_0(\Theta)$
P_y	$\frac{2\sqrt{2}}{3\sigma_0(\Theta)}Im\sum_{m_d}[(t_{1,0,1,m_d}+(-1)^i t_{0,0,1,m_d})^* t_{1,1,1,m_d}+t^*_{1,-1,1,m_d}(t_{1,0,1,m_d}+(-1)^{i-1}t_{0,0,1,m_d})]$
T	$Im(\sum_{s,m_s}(t^*_{s,m_s,1,-1}t_{s,m_s,1,0}+t^*_{s,m_s,1,0}t_{s,m_s,1,1})/\sigma_0(\Theta))$
C_x	$\frac{2\sqrt{2}}{3\sigma_0(\Theta)}Re\sum_{m_d}[(t_{1,0,1,m_d}+(-1)^i t_{0,0,1,m_d})^* t_{1,1,1,m_d}+t^*_{1,-1,1,m_d}(t_{1,0,1,m_d}+(-1)^{i-1}t_{0,0,1,m_d})]$
E	$\frac{1}{2}\sum_{s,m_s}(\|t_{s,m_s,1,1}\|^2-\|t_{s,m_s,1,-1}\|^2)/\sigma_0(\Theta)$
F	$-Re\sum_{s,m_s}(t^*_{s,m_s,1,-1}t_{s,m_s,1,0}+t^*_{s,m_s,1,0}t_{s,m_s,1,1})/\sigma_0(\Theta)$
G	$Im\sum_{s,m_s}(t^*_{s,m_s,1,1}t_{s,m_s,1,-1})/\sigma_0(\Theta)$
T_{11}	$Im\sum_{s,m_s}(t^*_{s,m_s,1,-1}t_{s,m_s,-1,0})/\sigma_0(\Theta)$
T_{1-1}	$-Im\sum_{s,m_s}(t^*_{s,m_s,1,1}t_{s,m_s,-1,0})/\sigma_0(\Theta)$

In pion photoproduction the amplitudes T_{11} and T_{1-1} are related to observables P and H respectively. In deuteron disintegration case, due to two spin 1/2 particles in the final state there is no such direct relation. Since P here has nothing to do with recoil polarisation P we omit meson photoproduction notation for these two variables to avoid confusion.

the $N^*(1680)5/2^+$, which can be excited in photoproduction from the nucleon by the same multipoles and spin configurations as the d^* i.e. $E2$ and $M3$. The former would relate to the $A_{3/2}$ amplitude, while the latter requires a spin-flip and will mostly be seen in $A_{1/2}$. The $N^*(1680)5/2^+$ photoproduction on the proton is fully dominated by the $A_{3/2}$, hence it is not very informative for our case, while the $N^*(1680)5/2^+$ on the neutron has similar strength for both helicity amplitudes. The effect of $N^*(1680)5/2^+$ on beam-target and single target observables using the most recent Mainz MAID PWA solution for $\gamma n \to n\pi^0$ with Bonn and $N^*(1680)5/2^+$ terms only is shown in Fig 6(left). Strong effects are suggested in the E, T and $H(T_{11}/T_{1-1})$ observables for this d^*-analagous case. For the $p\pi^0$ case (Fig 6 right) the $E2 : M3$ ratio is expected to be 10:1 (compared to 1:1 with $n\pi^0$) so comparison of the two figures gives some indication about the sensitivity of the observables to multipolarities. From these studies it is suggested that the strong signal in $H(T_{11}/T_{1-1}$ in deuteron case) remains unchanged regardless of the multipolarity decomposition, while G shows more sensitivity and changes sign. The predictions for T show structures around 90 degrees in the regions indicated in Fig 4. However, with all the above interpretations it worth noting that the studies are only indicative for the d^* case, since background in the d^* region could influence the predictions.

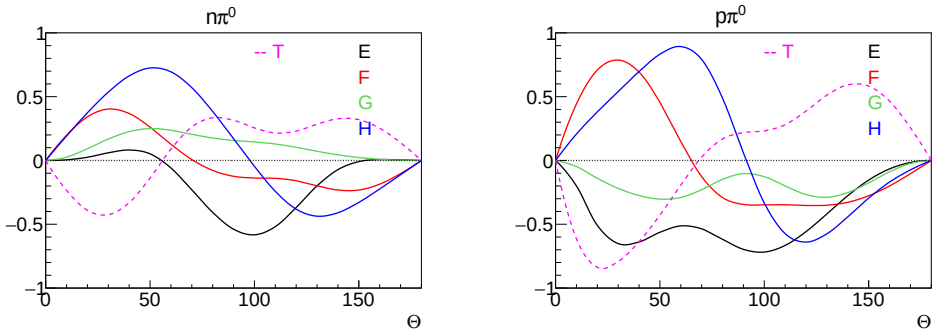

Figure 6: MAID predictions for photoexcitation of the $N^*(1680)$ (along with background from Born terms only). The predictions of various single- and double-polarisation observables for the $n\pi^0$ reaction (left) and $p\pi^0$ reaction (right) are shown. Photon energy = 1035 MeV (W=1680 MeV).

5 Experimental apparatus

5.1 Photon beam

The A2 photon beam is derived from the production of Bremsstrahlung photons during the passage of the MAMI electron beam through a thin diamond/amorphous radiator. The resulting photons can be circularly polarised, with the application of a polarised electron beam, or linearly polarised, in the case of a crystalline radiator. The degree of polarisation achieved is dependent on the energy of the incident photon beam and the energy range of interest. For the d^* energies (∼450-650 MeV), linear photon polarisations between 0.3 and 0.5 are feasible (Fig. 7). The Glasgow-Mainz Photon Tagger provides energy tagging of the photons by detecting the post-radiating electrons and can determine the photon energy with a resolution of 2 to 4 MeV depending on the incident beam energy. Each counter can operate reliably to a rate of ~ 3 MHz. Details on the updated Glasgow tagger can be found in Ref.[56]

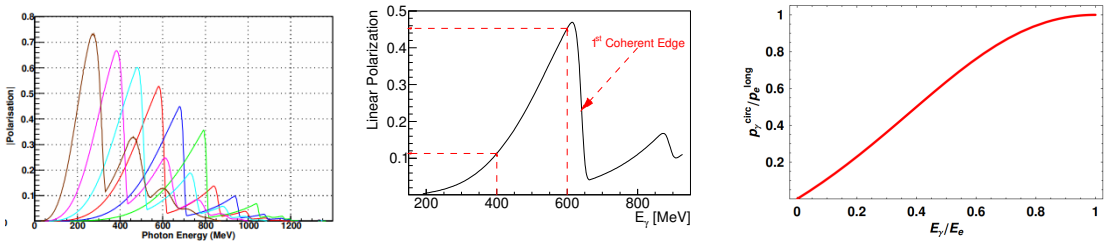

Figure 7: Linear polarisation available with the current collimation system for a variety of crystal orientations(left). Helicity transfer from the electron to the photon beam as function of the energy transfer(right). The MAMI beam polarisation is $P_e = 85\%$. Linear polarisation from the Aug2016 d^* beamtime(middle).

5.2 Polarised Deuterium target

A polarised frozen spin deuterated butanol (C_4D_9OD) target, contained within a horizontal 3He/4He dilution refrigerator will be employed. The deuterons will be dynamically polarised in a high magnetic field typically up to 80%. The target polarisation will be measured by an NMR system with a precision of 1.5%. During the measurements, the polarisation will be maintained in the frozen spin mode by an internal superconducting "holding coil". Relaxation times of more than 1000 hours could be reached and the polarisation will be refreshed once a week. The polarisation direction of the deuterons will be switched multiple times during a beam time, to reduce systematic effects in the data. Details on polarised deuteron target performance can be found elsewhere [47]. Recently, a deuteron polarisation $P_D = 80\%$ was obtained with Trityl doped butanol targets at 2.5 T magnetic field in a 3He/4He dilution refrigerator. The filling factor for the $\approx 2mm$ diameter butanol spheres into the 2 cm long, 2 cm diameter target container will be around 60%. The experience obtained from previous runs shows that, with a total tagged photon flux of $5 \cdot 10^7$, relaxation times of more than 1000h should be expected. The polarisation has to be refreshed by microwave pumping every two days. In conclusion, we estimate that we will achieve the following target parameters:

- Maximum total tagged photon flux in the energy range of 4 - 95% E0: $I_\gamma \approx 5 \cdot 10^7 \gamma/s$, with relaxation time of 1000 hours.
- Average target polarisation $P_d = 70\%$
- Target deuteron density in 2 cm cell: $n_T \approx 9.4 \cdot 10^{22} cm^{-2}$ (including dilution and filling factors)

5.3 Crystal Ball Detector System

The central detector system consists of the Crystal Ball calorimeter combined with a barrel of scintillation counters for particle identification and two coaxial multiwire proportional counters for charged particle tracking. This central system provides position, energy and timing information for both charged and neutral particles in the region between 21° and 159° in the polar angle, θ, and over almost the full azimuthal (ϕ)

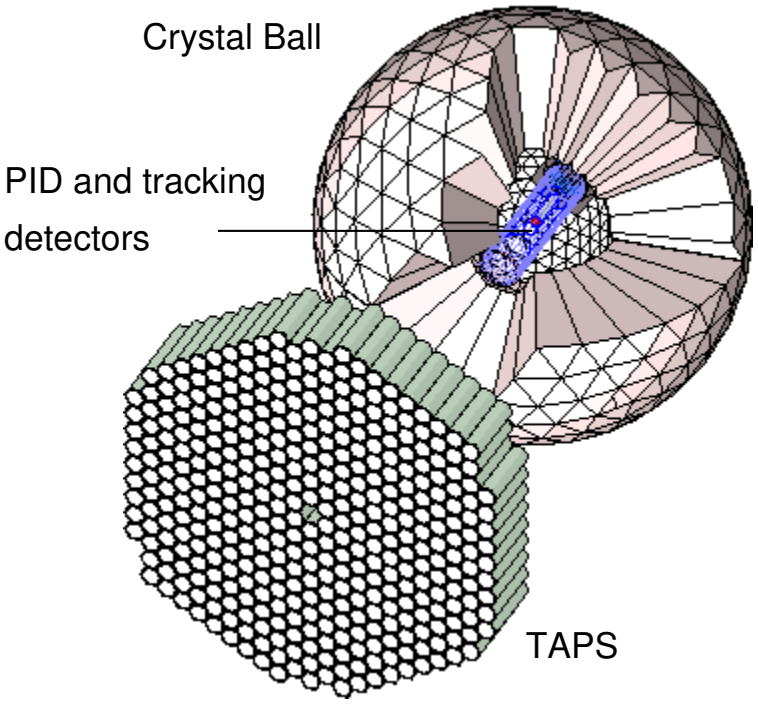

Figure 8: The A2 detector setup: the Crystal Ball calorimeter with cut-away section showing the inner detectors and the TAPS forward wall.

range. At forward angles, less than 21°, reaction products are detected in the TAPS forward wall. The full, almost hermetic, detector system is shown schematically in Fig. 8.

In order to distinguish between neutral and charged particles species detected by the Crystal Ball, the system is equipped with PID 2: a barrel detector of twenty-four 50-mm long 4-mm thick scintillators, arranged so that each PID 2 scintillator covers an angle of 15° in ϕ. By matching a hit in the PID 2 with a corresponding hit in the CB, it is possible to use the locus of the ΔE–E combination to identify the particle species (Fig. 9). This is primarily used for the separation of charged pions, electrons and protons. The PID 2 covers polar angles between 15° and 159°.

The excellent CB position resolution for photons stems from the fact that a given photon triggers several crystals and the energy-weighted mean of their positions locates the photon position to better than the crystal pitch. For charged particles, which deposit their energy over only one or two crystals, this is not so precise. Here the tracks of charged particles emitted within the angular and momentum acceptance of the CB detector will be reconstructed from the coordinates of point of intersections of the tracks with two

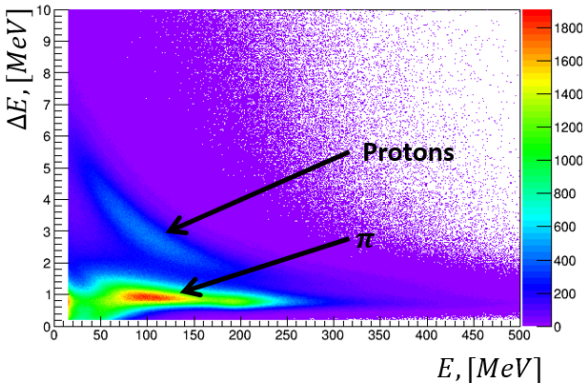

Figure 9: A typical ΔE/E plot from the PID detector. The upper curved region is the proton locus, the lower region contains the pions and the peak towards the origin contains mostly electrons.

coaxial cylindrical multiwire proportional chambers (MWPCs) with the cathode strip readout [17].

A mixture of argon (79.5%), ethane (30%) and freon-CF_4 (0.5%) is used as the filling gas in the MWPC. This mixture is a compromise between charge multiplication and localization requirements imposed by the ionizing particle tracks. Within each chamber both the azimuthal and the longitudinal coordinates of the avalanche will be evaluated form the centroid of the charge distribution induced on the cathode strips. The location of the hit wires(s) will be used to resolve ambiguities which arise from the fact that each pair of inner and outer strip cross each other twice. The expected angular resolution (rms) will be 2° in the polar emission angle ϑ and 3° in the azimuthal emission angle φ.

5.4 TAPS Forward Wall

The TAPS forward wall is composed of 384 BaF_2 elements, each 25cm in length (12 radiation lengths) and hexagonal in cross section, with a diameter of 59 mm. Every TAPS element is covered by a 5 mm thick plastic veto scintillator. The single counter time resolution is $\sigma_t = 0.2$ ns. The energy resolution can be described by the $\Delta E/E = 0.018 + 0.008/(E[GeV])^{0.5}$ [47]. The angular resolution in the polar angle is better than 1°, and in the azimuthal angle it improves with increasing θ, being always better than 1/R radian, where R is the distance in centimetres from the central point of the TAPS wall surface to the point on the surface where the particle trajectory meets the detector. The TAPS readout was custom built for the beginning of the CB@MAMI program and is effected in such a way as to allow particle identification by Pulse-Shape Analysis (PSA), Time-of-Fight (TOF) and ΔE/E methods (using the energy deposit in the plastic scintillator to give ΔE). TAPS can also contribute to the CB multiplicity trigger and is currently divided into six sectors for this purpose. The inner two rings of the detector wall have recently been replaced with lead tungstate crystals to enable higher rate capability.

6 Data analysis

The analysis of the data is rather straightforward and clean separation of the $d(\gamma, pn)$ channel with deuteron target CB data has been established in our previous analysis [45], where the beam spin asymmetry data and cross section data gave agreement with previous data within statistical and systematic errors. The $d(\gamma, pn)$ events of interest contain a proton track and an uncharged (neutron) hit. The proton will be identified using the correlation between the energy deposits in the PID and CB using ΔE - E analysis, Fig. 9. The proton identification also required an associated charged track in the MWPC. The neutron candidates comprised uncharged hits in the CB, which did not have any associated MWPC or PID signal. The neutron angles will be determined using the CB hit with production vertex coordinates defined by the intercept of the photon beam trajectory and the associated charged (proton) track. Once the candidate proton and neutron tracks are identified, a kinematic fit will be employed to increase the purity of the event sample and to improve the accuracy of the determination of the reaction kinematics. To fully constrain the kinematics of the $d(\gamma, pn)$ reaction at a given incident photon energy, two kinematic quantities are required. The angles of both proton and neutron as well as the proton energy are measured, enabling an overconstrained kinematic fit analysis. A 10% probability cut will be employed to select the events of interest, Fig.11. The neutron detection efficiency of the CB ($\sim 30\%$) was determined in a dedicated measurement, Ref. [48] and can be easily reproduced by simulation. Neutron detection efficiency drops at lower energies, and thus reactions with backward going neutrons (forward going protons) are somewhat statistically suppressed (see Fig. 10).

The T, F and T_{11}/T_{1-1} observables will be determined from asymmetries in beam and/or target polarisation orientations and therefore, detector efficiencies do not play a crucial role in the analysis. This benefit is optimised if analysis is done in event-by-event likelihood way as we envisage. We recently developed [54] such methods in analysis of beam-target observables and would plan to adopt similar procedures in the proposed analysis.

For the beam target observables we will follow the procedure adopted previously [47]. The cross section for photoreactions with linearly polarised photons on a transversely polarised deuterium target is given by:

$$d\sigma/d\Omega = \sigma_0 \cdot P_\gamma^L P_T (T_{11} \sin(2(\alpha-\phi)) \cos(\beta-\phi) + T_{1-1} cos(2(\alpha-\phi)) sin(\beta-\phi)) \quad (2)$$

where σ_0 is the unpolarised cross section, P_γ^L is the polarisation of the beam, P_T the degree of polarisation of the target, T_{11} and T_{1-1} are the polarisation observables defined in Table 2, ϕ is proton azimuthal angle

and α (β) are azimuthal angle of the photon beam polarisation plane in the $\parallel$ setting (the azimuthal angle of the target polarisation vector in the $\Uparrow$ settings) respectively.

For a circularly polarised beam on a transversely polarised target the cross section is given by:

$$\frac{d\sigma}{d\Omega} = \sigma_0(1 + P_T cos(\phi) P_\gamma^\odot F + P_T sin(\phi) T) \tag{3}$$

where $P_\gamma^\odot$ is the degree of circular polarisation of the beam and F, T are the polarisation observables defined in Table 2.

The different observables $(T, F, H, T_{11}, T_{1-1})$ can be extracted from asymmetries constructed according to the cross section dependencies above. The extraction of F observable requires both beam and target polarisation and can be extracted from following asymmetry:

$$F\cos(\phi) = \frac{1}{P_T P_\gamma^\odot} \frac{(N^+ - N^-)}{(N^+ + N^-)} \frac{1}{d} \tag{4}$$

where N denotes the count rate, d is the dilution factor of the target and $\pm$ superscripts correspond to the helicity state of the incoming photon beam. The T observable can be extracted from the asymmetry (taking equal flux of beam polarisation states to create an effectively unpolarised beam):

$$T sin(\phi) = \frac{1}{P_T} \frac{(N^\Uparrow - N^\Downarrow)}{(N^\Uparrow + N^\Downarrow)} \frac{1}{d} \tag{5}$$

where the $\Uparrow$ and $\Downarrow$ superscripts correspond to the target spin directions.

It was recently shown that a likelihood analysis for polarisation observables provide the same results as direct asymmetry reconstruction but has much lower bias and also less sensitive to acceptance effects [54]. The procedure was well established in CLAS collaboration on various E, C_x, G, etc... observables. Due to multiple polarisation constrains linear/circular photon polarisation and $\Uparrow$ / $\Downarrow$ target polarisations in proposed beamtime, an event-by-event likelihood analysis is expected to perform better than conventional asymmetry methods. All data analysis proposed in this note will be performed using likelihood methods. We also plan to perform cross-check of observables extraction using asymmetry methods for a simplest variable only (T).

6.1 Dilution factors

The polarised target contains not only deuterons but also unpolarised carbon/oxygen nuclei. This dilution means that additional measurements using a carbon foam target are necessary to determine the so-called dilution factor (d) given by:

$$d(W, \cos(\theta)) = 1 - \frac{N_{C/O}(W, \cos(\theta))}{N_{target}(W, \cos(\theta))}. \tag{6}$$

where W is the centre-of-mass energy of the bin and θ is the angle of the final state nucleon. For a fully polarised target without C/O contribution the dilution factor would be 1. More information about dilution factor and C/O background subtraction routinely employed at A2 can be found in Ref [52].

6.2 Trigger conditions

To better optimise the rate of deuterium photodisintegration event collection, we propose to use an M2 trigger instead of M1. However, during the run we will additionally operate a highly prescaled M1 trigger to provide data for systematic studies. The analysis will not utilise TAPS (as done for the beam spin asymmetry analysis of Ref. [45])because events with TAPS kinematics cannot be measured exclusively (if one of the particles from a deuterium photodisintegration event goes into TAPS, the corresponding particle would occur at very backward angles with extremely small energy below or close to detector thresholds. For such events a reconstruction of $d(\gamma, p)n$ and/or $d(\gamma, n)p$ events is possible, but sufficient background suppression is not. Also, these events occupy up to 1/3 of the data stream due to low event selectivity, while covering only a small fraction of the event kinematics (see Fig. 12 where such events are excluded).

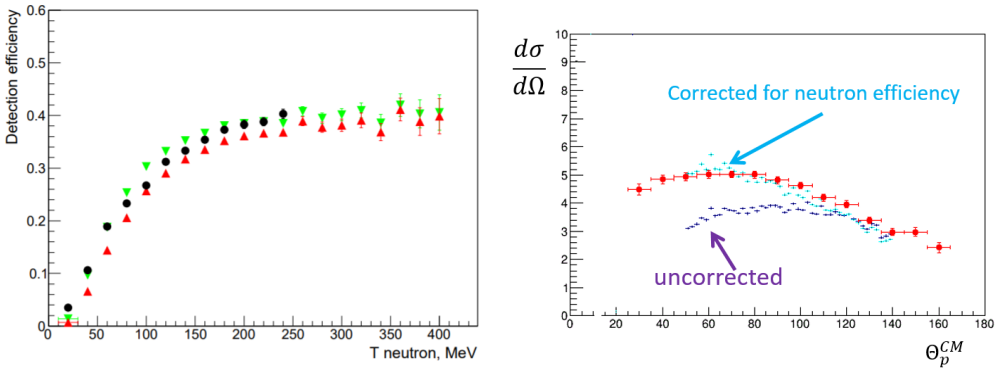

Figure 10: A neutron efficiency as a function of neutron energy for the CB detector from Ref. (left) and the effect of neutron efficiency on reconstructed differential observables(right). Red data shows published differential distributions from Ref. [48]

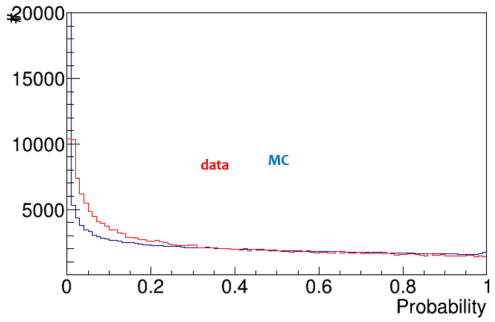

Figure 11: A probability distribution function for the kinematical fit selection based on Mar13 data $d(\gamma, pn)$.

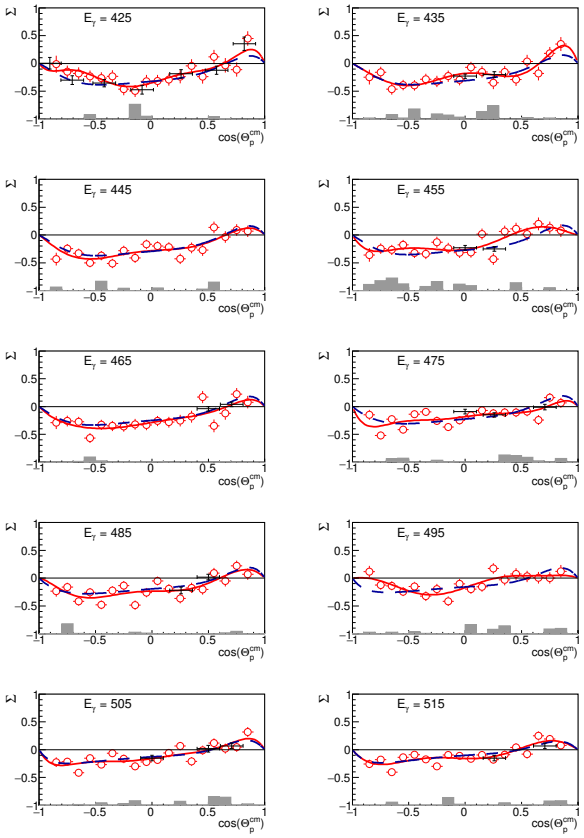

Figure 12: Beam spin asymmetry (Σ) results from Aug2016 experiment (red open circles) in comparison with previous results (black crosses) [49, 50]. The corresponding systematic uncertainties are depicted as shaded bars on the bottom. Energy independent (energy dependent) Legendre polynomial fits are shown as solid red(dashed blue) lines (see Ref. [45] for details).

7 Expected statistics and beamtime request

To achieve a 1% statistical accuracy in the acquired data with a typical beam polarisation ($P_\gamma \sim 0.4$) and target polarisation ($P_T \sim 0.7$) requires a number of events per bin (N) of:

$$N = \frac{1.0}{P_T^2 P_\gamma^2 \delta A^2} \sim 100k \tag{7}$$

Taking $P_T = 0.7$, $P_\gamma = 0.4$ and $\delta A = 1\%$. The countrate (N/s) can be evaluated as

$$N/s = I \cdot n_T \cdot \epsilon \cdot \sigma \sim 1s^{-1} \tag{8}$$

the flux (I) within a ± 15 MeV photon energy in the d^* region is $I = 10^7\gamma/s$ on the target), calculated assuming a rate at the exit of the tagger of 1.5 MHz/MeV and a tagging efficiency of 0.23 corresponding to a 2mm photon beam collimator. The number of deuterium nuclei in the target is $n_T = 9.6 \cdot 10^{22} cm^{-2}$, the detection efficiency for pn final state is $\epsilon = 0.2$ (corresponding to a 70% efficiency for protons and 30% efficiency for neutrons) and the disintegration cross section (in the region of the d^* is $\sigma = 5 \cdot 10^{-30} cm^2$. Therefore a total beamtime of 7 weeks is required to achieve the intended statistical accuracy within each photon energy bin.

Table 3: Expected beamtime length

Target	Radiator	Beam polarisation	Target polarisation	days
D-butanol	Diamond	$\parallel$	$\Uparrow$	7
D-butanol	Diamond	$\parallel$	$\Downarrow$	7
D-butanol	Diamond	$\perp$	$\Uparrow$	7
D-butanol	Diamond	$\perp$	$\Downarrow$	7
D-butanol	Moeller	$\odot/\otimes$	$\Uparrow$	3
D-butanol	Moeller	$\odot/\otimes$	$\Downarrow$	3
Carbon	Diamond	$\parallel$	–	3
Carbon	Diamond	$\perp$	–	3
				6 weeks

The total beamtime request, according to the estimate above, is outlined in Table 3. The beamtime with elliptically polarised photons is split into two different orientations of the polarised target. In addition we request a small period of running with purely circularly polarised beam, to provide systematic checks of observables extracted using equal amounts of linearly polarised beam.

The following number needs to be further subdivided by two polarisation states of a target ($\Uparrow$ / $\Downarrow$) and four states of a beam ($\parallel$/ $\perp$) from diamond radiator and "unpolarised" ($\odot/\otimes$) from amorphous radiator. The use of elliptically polarised photon beam allows simultaneous measurement of ($\odot/\otimes$) with linear polarised $\parallel$ or $\perp$ beam. This has been studied in a number of previous MAMI analyses [47]. A separate measurement employing a carbon target will also be obtained to enable analysis of events originating from unpolarised nuclei (Carbon, Oxygen) in the butanol target. The necessary beamtime to achieve the proposed measurement is summarised in the table below.

An extra 1 week (without beam) is required to setup polarised target in the A2 hall.

References

[1] J. Chadwick, M. Goldhaber, Nature **134**, 237, (1934).

[2] M. Bashkanov *et al.*, Phys. Rev. Lett. **102**, 052301, (2009).

[3] P. Adlarson *et al.*, Phys. Rev. Lett. **106**, 242302, (2011).

[4] P. Adlarson *et al.*, Phys. Lett. B **721**, 229, (2013).

[5] P. Adlarson *et al.*, Phys. Rev. C **88**, 055208, (2013).

[6] P. Adlarson *et al.*, Phys. Lett. B **743**, 325, (2015).

[7] P. Adlarson *et al.*, Eur. Phys. J. A **52**, 147, (2016).

[8] P. Adlarson *et al.*, Phys. Rev. Lett. **112**, 202301, (2014).

[9] P. Adlarson *et al.*, Phys. Rev. C **90**, 035204, (2014).

[10] I. Vidaña Hyperon puzzle, Proceedings of the Royal Society A474, 20180145

[11] I. Vidaña, M. Bashkanov, D.P. Watts, A. Pastore, Phys. Lett. B **781**, 112-116, (2018).

[12] A. Mantziris, I. Vidaña, M. Bashkanov, D.P. Watts, A. Pastore, A.M. Romero, arXiv:2002.06571.

[13] Ben Margalit and Brian D. Metzger, Astrophys.J. 850, no.2, L19 (2017)

[14] M. Bashkanov *et al.*, arXiv:1911.08309

[15] M. Bashkanov and D.P. Watts, J. Phys G **47**, no.3, 03LT01, (2020)

[16] M. Bashkanov and D.P. Watts, Phys. Rev. C **100**, no.1, 012201, (2019)

[17] R. Crawford *et al.* Nucl. Phys. A **603**, 303-325, (1996).

[18] H. Ikeda *et al.*, Phys. Rev. Lett. **42**, 1321, (1979).

[19] K. Wijesooriya *et. al* Phys. Rev. Lett., **86**, 2975, (2001)

[20] T. Kamae, T. Fujita. Phys. Rev. Lett. **38**, 471 (1977).

[21] P. Demorest, T. Pennucci, S. Ransom, M. Roberts, J. Hessels, Nature **467**, 1081 (2010).

[22] J. Antoniadis *e*t al., Science **340** 6131(2013).

[23] E.Annala *et al.*, arXiv:1711.02644v1

[24] M. Guenther, Master Thesis, University of Basel (2015); PoS (Hadron2017) 051.

[25] T. Ishikawa *et al.*, Phys. Lett. B **772**, 398, (2017).

[26] M. Bashkanov, H. Clement, T. Skorodko, Eur. Phys. J. A **51**, 7, 87, (2015).

[27] D.E. Frederick Phys. Rev. **130**, 1131, (1963).

[28] W. Bertozzi *et. al* Phys. Rev. Lett. **10**, 106, (1963).

[29] M. Hugi, *et al.* Nucl.Phys. **A472**, 701, (1987).

[30] J.M. Cameron *et al.* Nucl.Phys. **A458**, 637-651, (1986).

[31] D.P. Watts, J.R.M Annand, M. Bashkanov, D.I Glazier, MAMI Proposal Nr. A2/03-09, `http://bamboo.pv.infn.it/Mambo/MAMI/prop_2009/MAMI-A2-03-09.pdf`

[32] M. H. Sikora *et al.* Phys. Rev. Lett. **112**, 022501, (2014).

[33] K.-H. Kaiser *et al.*, Nucl. Instr. Meth. A **593**, 159, (2008).

[34] J.C. McGeorge *et al.*, Eur. Phys. J. A **37**, 129, (2008).

[35] A. Starostin *et al.*, Phys. Rev. C **64**, 055205, (2001).

[36] S.J.D. Kay, Ph.D. thesis, University of Edinburgh, 2018, `https://www.era.lib.ed.ac.uk/handle/1842/31525`.

[37] G. Audit *et al.* Nucl. Instr. Meth. A **301**, 473, (1991).

[38] M. Bashkanov *et al.* to be published.

[39] SAID data base `http://gwdac.phys.gwu.edu/`; R. A. Arndt *et al.*, Phys. Rev. C **76**, 025209 (2007).

[40] S.Agostinelli *et al.*, Physics Research **A 506**, 250-303, (2003).

[41] Y. Kang, (1993), Ph.D. thesis Bonn

[42] A.S. Bratashevskiĭ *et al.* Pis'ma Zh. Eksp. Teor. Fiz. **31**, 295, (1980).

[43] Liu F. F., Lundquist D. E., and Wiik B. H.,Phys. Rev. **165**, 1478, (1968).

[44] J. Babcock and J.L. Rosner, Annals of Physics **96**, 19, (1976).

[45] M. Bashkanov *et al.*, Phys. Lett. B**789**, 7, (2019).

[46] M. Bashkanov, H. Clement, T. Skorodko, Nucl.Phys. A**958**, 129-146, (2017).

[47] F.Afzal, PhD thesis, University of Bonn, 2019

[48] M. Martemianov *et al.* JINST **10**, no.04, T04001, (2015).

[49] F. V. Adamian *et al.* Jour. Phys. G 17(8):1189, (1991).

[50] V.G. Gorbenko *et al.* Nucl. Phys. A**381**, 330, (1982).

[51] S. Wartenberg *et al.* Few-Body Systems **26**, 213 (1999).

[52] L. Witthauer *et al.* Phys.Rev.Lett. **117**, no.13, 132502, (2016)

[53] A. Fix and M. Ostrick, private communications.

[54] N. Zachariou, Few Body 24 (2019); T. Cao, PhD thesis, University of South Carolina (2016), `https://www.jlab.org/Hall-B/general/thesis/TCao_thesis.pdf`

[55] Y. Ohashi, *et al.*, Phys.Rev. C**36**, (1987), no.6, 2422

[56] C. McGeorge (Glasgow), A2 collaboration meeting 04/2018, `https://a2wiki.kph.uni-mainz.de/intern/daqwiki/_media/meetings/collaboration_meetings/2018_04/a2_2018-04_mcgeorge.pdf`